POLYPUBLIE
Polytechnique Montréal

POLYTECHNIQUE
MONTRÉAL

UNIVERSITÉ
D'INGÉNIERIE

Titre: Title:	VUV Photodeposition of Thiol-Terminated Films: A Wavelength-Dependent Study
Auteurs: Authors:	Evelyne Kasparek, Jason Robert Tavares, Michael R. Wertheimer et Pierre-Luc Girard-Lauriault
Date:	2018
Type:	Article de revue / Journal article
Référence: Citation:	Kasparek, E., Tavares, J. R., Wertheimer, M. R. & Girard-Lauriault, P.-L. (2018). VUV Photodeposition of Thiol-Terminated Films: A Wavelength-Dependent Study. *Langmuir*, *34*(41), p. 12234-12243. doi:10.1021/acs.langmuir.8b01691

Document en libre accès dans PolyPublie
Open Access document in PolyPublie

URL de PolyPublie: PolyPublie URL:	https://publications.polymtl.ca/3687/
Version:	Version finale avant publication / Accepted version Révisé par les pairs / Refereed
Conditions d'utilisation: Terms of Use:	Tous droits réservés / All rights reserved

Document publié chez l'éditeur officiel
Document issued by the official publisher

Titre de la revue: Journal Title:	Langmuir (vol. 34, no 41)
Maison d'édition: Publisher:	ACS Publications
URL officiel: Official URL:	https://doi.org/10.1021/acs.langmuir.8b01691
Mention légale: Legal notice:	"This document is the Accepted Manuscript version of a Published Work that appeared in final form in Langmuir, copyright © American Chemical Society after peer review and technical editing by the publisher. To access the final edited and published work see https://doi.org/10.1021/acs.langmuir.8b01691"

VUV Photo-deposition of Thiol-terminated

Films - A Wavelength-dependent Study

Evelyne Kasparek [a]*, Jason R. Tavares* [b]*, Michael R. Wertheimer* [c]*, Pierre-Luc*

Girard-Lauriault [a] *

[a]Plasma Processing Laboratory, Department of Chemical Engineering,

McGill University, Montreal, QC H3A 2B2, Canada

[b]Photochemical Surface Engineering Laboratory, Department of Chemical

Engineering, École Polytechnique de Montréal, Montréal, QC H3C 3A7, Canada

[c]Groupe des couches minces (GCM) and Department of Engineering Physics,

École Polytechnique de Montréal, Montréal, QC H3C 3A7, Canada

1

ABSTRACT

Photo-initiated chemical vapor deposition (PICVD) has become attractive for selective and specific surface functionalization, since it relies on a single energy source, the photons, to carry out (photo-) chemistry. In the present wavelength (λ)-dependent study, thiol (SH)-terminated thin film deposits have been prepared from gas mixtures of acetylene (C_2H_2) and hydrogen sulfide (H_2S) via PICVD using four different vacuum-ultraviolet (VUV) sources, namely KrL (λ_{peak}=123.6 nm), XeL (λ_{peak} =147.0 nm), XeE (λ_{peak} =172.0 nm) and Hg (λ=184.9 nm) lamps. Different λ influence the deposition kinetics and film composition, reflecting that photolytic reactions are governed by the gases' absorption coefficients, $k(\lambda)$. Thiol concentrations, [SH], up to ~7.7 %, were obtained with the XeL source, the highest reported in the literature so far. Furthermore, all films showed island-like surface morphology, irrespective of λ.

INTRODUCTION

General introduction

Synthetic polymers are broadly used in biomaterials due to their favorable bulk properties, such as high mechanical stability and elasticity, non-toxicity, and low degradation in the human body.[1-2] Nevertheless, their surfaces are generally chemically inert and show poor biocompatibility, leading to inadequate interactions with cells, generating strong foreign body reactions such as inflammation, clotting and infection.[3-5] Therefore, commercial polymers must often undergo surface functionalization, which will aid their surfaces to adapt to biological demands by

2

immobilizing biomolecules onto the polymers. The principal methods of immobilizing a biomolecule to a polymeric surface are adsorption via electrostatic interactions, ligand-receptor pairing, and covalent attachment. Non-covalent adsorption can be desirable for certain applications (e.g. in drug delivery), and there is broad evidence in the literature that nitrogen (N)- and oxygen (O)-containing functional groups, more specifically primary amines (-NH2) and carboxylic acid (-COOH) or hydroxyl (-OH) functionalities, respectively, are often advantageous in promoting protein and cell adhesion via non-covalent adsorption.[6-9] However, covalent immobilization of biomolecules has been shown to be superior by providing a stable bond between the biomolecules and the functionalized surface, extending the shelf-life of the biomolecule, and allowing for continued bioactivity.[2, 10] Sulfur (S)-rich, more specifically thiol (SH)-terminated surfaces offer excellent platforms for covalent immobilization of biomolecules through specific and selective thiol-ene coupling reactions. This coupling reaction has been widely exploited for the construction of immobilized antibodies, enzymes and peptides.[11-16]

So far, SH-terminated surfaces have been mainly synthesized through tedious, non-specific, multi-step wet-chemical approaches, often involving various toxic and expensive solvents.[14-16] Over the last decade, the synthesis of SH-terminated surfaces has been also accomplished through plasma-enhanced chemical vapor deposition (PECVD) techniques using single-molecule precursors (e.g. allylmercaptan,[17-18] propanethiol[19-21]) and more recently, using gas mixtures comprising a hydrocarbon (either ethylene or butadiene) and hydrogen sulfide (H2S).[22] Plasma-based techniques offer several benefits over the wet-chemical ones,

3

such as low processing temperatures, no solvent requirement, and fast reaction times. Despite these advantages, the reactions occurring in a plasma are difficult to control since the main originators of chemical reactions, "hot" electrons, possess a broad, Maxwell-Boltzmann-like energy distribution,[9, 23] thereby making the reactions non-specific and non-selective.

More recently, photo-initiated CVD (PICVD) techniques have emerged. This method has been studied extensively and it has established a firm position as a CVD method capable of producing high quality, functional thin films, often comparable to traditional plasma CVD.[24-28] In PICVD, the energy required to induce reactions leading to deposition is provided by photons. Therefore, only one energy component carries out (photo-) chemistry, potentially allowing for better control of the overall process compared to plasma counterparts. To obtain thin films from specific precursors, absorption of photons by the precursors must be significant, and photon energies must be sufficiently high to overcome bond dissociation energies, D_0, to induce photo-dissociation.[29] Therefore, photo-absorption by molecules as a function of wavelength, $k(\lambda)$, must be considered for successful photo-induced deposition.[26] Almost all of the observed absorption continua correspond to dissociation processes; by choosing a specific photon wavelength, λ, different dissociation products can be generated. Wavelength dependency has been observed for deposition kinetics and film quality.[30-31] Nevertheless, selectivity in excitation has not been fully exploited so far, partly due to a lack of available light sources and other required equipment. This is of high importance since it could aid in selectively designing thin film deposits by simply using different λ values.[9, 23, 27-28, 32]

4

In our previous study,[22] we synthesized SH-terminated coatings using ethylene

(C_2H_4)/H_2S and butadiene (C_4H_6)/H_2S gas mixtures with a single non-coherent VUV

source (λ_{KrL} = 123.6 nm). We obtained adjustable sulfur concentrations, [S], ranging

from 2 to 30 at.% and thiol concentrations, [SH], up to 1.75%. In the present work, we

broaden the experimental window by performing a λ-dependent deposition study of

SH-terminated coatings using variable gas mixture ratios, R, of acetylene (C_2H_2) and

H_2S and four different λ values, namely λ_{KrL} = 123.6 nm, λ_{XeL} = 147.0 nm, λ_{XeE} =

172.0 nm, and λ_{Hg} = 184.9 nm. In this context, we aimed to understand the growth

mechanisms of the synthesized SH-terminated films using PICVD, since only one

kind of excitation (VUV photons) at a specific wavelength is active and available for

initiating reactions. Besides determining the chemical composition of the coatings, the

deposition kinetics, film growth and -morphology were also studied. The dependence

of these as a function of λ was investigated in detail. By exploring a broader range of

photon energies, we intended to find an "ideal" combination of R and photon energy

which gives the highest [SH] values, thereby maximizing the possibilities for further

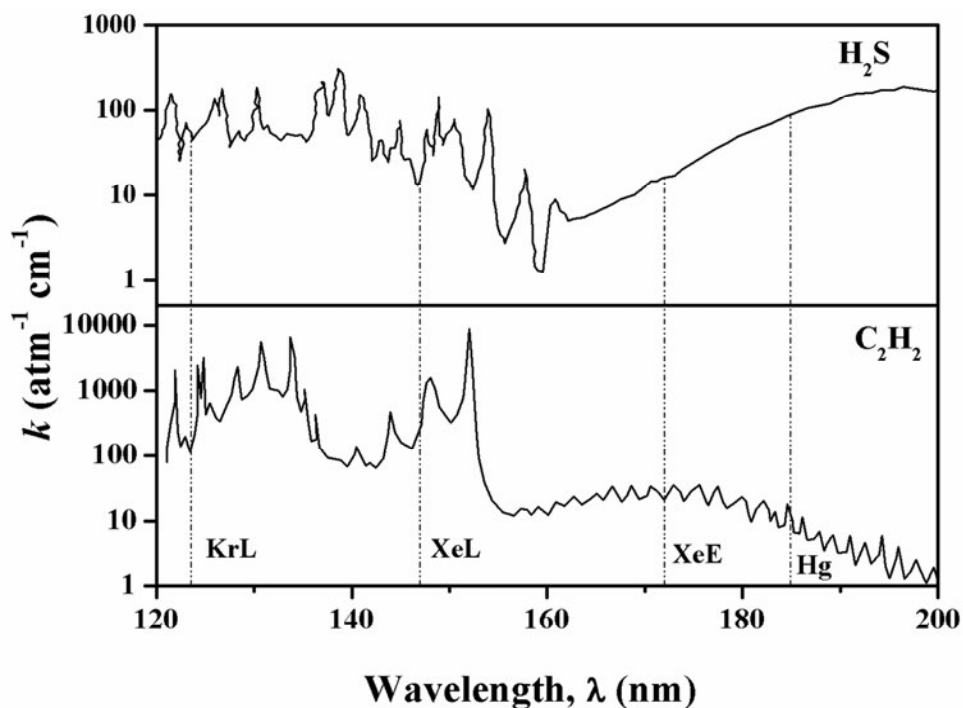covalent immobilization of biomolecules through thiol-ene coupling reactions.

Wavelength-dependent photolysis of C_2H_2 and H_2S

Figure 1. VUV-absorption, k (atm^{-1}cm^{-1}, base e) of gaseous H_2S[33] and C_2H_2[34]; the wavelengths, λ, of the VUV lamps used are also shown (λ_{KrL} = 123.6 nm, λ_{XeL} = 147.0 nm, λ_{XeE} = 172.0 nm, λ_{Hg} = 184.9 nm).

Activation and photo-dissociation of C_2H_2 and H_2S are expected from all four sources on account of their relatively strong absorption, $k(\lambda)$ (**Figure 1**), throughout the studied spectral range (123.6 $<\lambda<$ 184.9 nm). Nevertheless, the radiation from some lamps is more strongly absorbed by the two precursor gases than others, especially in the case of C_2H_2 (**Table 1**), and these differences should be reflected in the deposition behaviour of the films at different λ.

Table 1. Absorption coefficients, $k(\lambda)$, of H_2S[33] and C_2H_2[34] at the wavelengths, λ, of interest.

Lamp	Peak Wavelength, λ_{peak} (nm)	Absorption of C_2H_2, k_{C2H2} (atm^{-1}cm^{-1})	Absorption of H_2S, k_{H2S} (atm^{-1}cm^{-1})
KrL	123.6	112	48
XeL	147.0	303	15
XeE	172.0	35	16
Hg	184.9	9	92

Photo-dissociation of acetylene can occur upon absorption of photons with energies greater than 5.8 eV, or λ < 214 nm (**Figure 1**). Two primary processes have been identified to occur when C_2H_2 absorbs photons in the studied λ range:

(i) Direct dissociation:

$$C_2H_2 + h\upsilon \ (> 5.8 \ eV) \rightarrow C_2H \cdot + H \cdot \qquad \textbf{(1)}$$
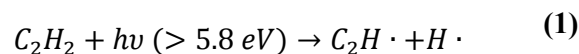
(ii) The formation of an excited metastable molecule, which has a relatively long lifetime ($\leq$ 1 ms) with respect to dissociation:[35-37]

$$C_2H_2 + h\upsilon \; (> 5.8 \; eV) \rightarrow C_2H_2^* \qquad \textbf{(2)}$$
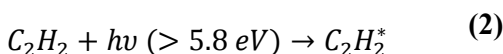
Formation of organic coatings can either occur through recombination of the created

radicals in reaction **(1)**, or through collisions of the metastable molecule with ground-

state C_2H_2 (excited molecule mode polymerization):[35, 38]

$$C_2H_2^* + C_2H_2 \; \rightarrow C_4H_4^* \qquad \textbf{(3)}$$

$$C_4H_4^* + \; C_2H_2 \rightarrow C_6H_6^* \, , etc. \qquad \textbf{(4)}$$
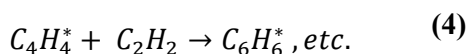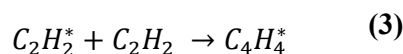
Collisions of an excited molecule with either the walls or ground-state C_2H_2 can lead

to chain-terminating reactions, but can also result in the formation of stable

molecules.

Although the same primary processes have been reported for all wavelengths

of interest, the quantum yields of reactions **(1)** and **(2)** depend not only on λ, but also

on pressure, *p*. The quantum yield is of interest, since it influences the route of coating

formation.[38-39] At λ=123.6 and 147.0 nm and low *p* (<106 Pa=0.8 Torr), the quantum

yield of reaction **(1)** is high, and direct dissociation is immediate.[34, 40-41] At low *p*,

continuous absorption of photons by the restricted number of C_2H_2 molecules leads to

direct dissociation. As *p* increases and more C_2H_2 molecules are available, the

creation of an excited state (reaction **(2)**) becomes more important since not all

molecules can continuously absorb the available photons. As reaction **(2)** becomes

more important, deactivation and/or collisions of the excited molecule with ground-

state C_2H_2 can lead to formation of major photochemical (stable) products, namely

8

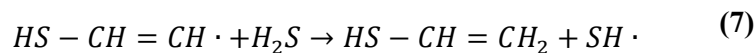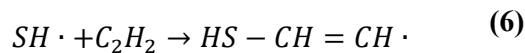diacetylene, ethylene, hydrogen, and small amounts of vinylacetylene and benzene.[40-42] At λ=172.0 and 184.9 nm and low p (<106 Pa=0.8 Torr), the quantum yield of reaction **(1)** was reported to be 1/5 as large as at the above-mentioned shorter λ values, indicating that direct dissociation is less important.[43] Therefore, deactivation of $C_2H_2^*$ at the reactor walls is more probable than further reactions that could lead to coating formation. With increasing p, more collisions occur, reaction **(1)** becomes more significant, and deactivation less relevant through higher probability of radical creation; thus, increased polymer formation can be observed.[43] Due to this particular photolytic behavior of C_2H_2, not only λ but also p needs to be considered in order to account for quantity of organic coating formation. Based on these theoretical considerations and experimental trials, a rather high p value (p=400 Pa=3 Torr) was chosen in this work as a compromise, so as to obtain appreciable coatings formation at all of the λ values investigated.

Hydrogen sulfide, H_2S, the second gaseous reagent in this study, strongly absorbs in the 120-250 nm VUV spectral range (**Figure 1**). Upon absorption at λ<309 nm, direct photolysis occurs, leading to cleavage of the H-SH bond:[44-45]

$$H_2S + h\upsilon \ (> 4.0 \ eV) \rightarrow SH \cdot + H \cdot \qquad \textbf{(5)}$$
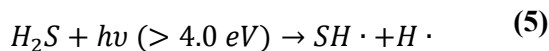
Reaction **(5)** has been identified as the primary process for all λ of interest. Secondary reactions include the formation of H and S through the reaction of the created radicals with each other or with H_2S.

Formation of polymer-like sulfur-rich thin films can occur through propagation of the excited state acetylenes (reactions **(2)** to **(4)**) or through thiol-yne chain reactions, initiated by the addition of SH· radicals, formed in reaction **(5)**, to acetylene:

$$SH \cdot + C_2H_2 \rightarrow HS - CH = CH \cdot \qquad \textbf{(6)}$$

$$HS - CH = CH \cdot + H_2S \rightarrow HS - CH = CH_2 + SH \cdot \qquad \textbf{(7)}$$

The product of reaction **(7)** can further react with SH· radicals forming even larger chains that can be incorporated into the organic coatings.

EXPERIMENTAL SECTION

VUV photo-polymerization

The experimental set-up used for VUV photo-chemical experiments (**Figure 2**) was based on the design developed by Truica-Marasescu et al.[23, 27-28, 32], and was similar to the one used in our earlier work.[22]
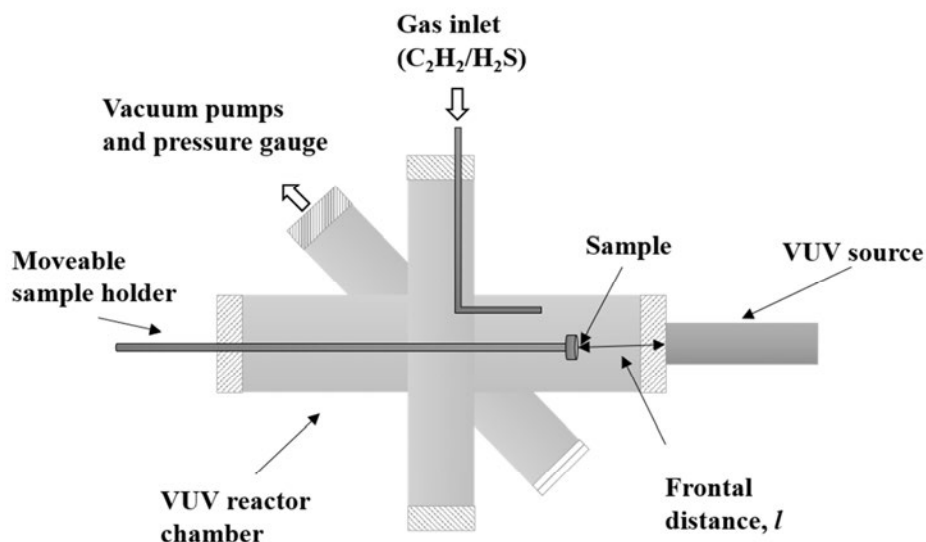
Figure 2. Cross section of the vacuum ultra-violet (VUV) photo-chemical reactor chamber used for depositing thiol-terminated organic thin films.

Briefly, it consisted of a stainless steel six-way cross chamber, evacuated to low p (base pressure $p < 10^{-6}$ Pa=7.5·10^{-9} Torr) using a turbo-molecular pump in tandem with a two-stage rotary vane pump. The operating pressure was maintained at p=400 Pa=3 Torr. The flow rate of the hydrocarbon, C_2H_2 (99.6%, MEGS Inc., Montreal, QC, Canada), $F_{(C2H2)}$, was kept constant at 10 sccm using a mass flow controller (Brooks Instruments, Hatfield, PA, USA), while that of H_2S (99.5%, MEGS Inc., Montreal, QC, Canada), $F_{(H2S)}$, was varied between 0 and 10 sccm; this yielded values of the gas mixture ratio R (=$\frac{F_{(H2S)}}{F_{(C2H2)}}$) ranging from 0 to 1. The purity of C_2H_2, which is commonly supplied dissolved in acetone in bottles filled with a porous medium,[46] was assured by connecting the reservoir to a C_2H_2 filter (Balston 95A-1/4 Acetylene Filter, Parker, Haverhill, MA, USA). The removal of acetone from C_2H_2 was important since acetone is photochemically active at the wavelengths used in this

11

study and could contribute to the formation of the organic coatings.[47] A removal

efficiency of 70 % was achieved with the above-mentioned filter. Polymer-like[48]

coatings resulting from the photo-chemical reactions, hereafter designated "UV-

PA:S" (for "ultraviolet-polymerized sulfurized acetylene"), were deposited on 500

μm-thick (100) p-type silicon wafers (University Wafer, Boston, MA,USA).

Four different VUV sources were used in the present λ-dependent study to

deposit UV-PA:S films, namely a low-pressure mercury (Hg) lamp (STER-L-RAY®,

Hauppauge, NY, USA) and three non-coherent commercial resonant or excimer noble

gas VUV lamps (Resonance Ltd., Barrie, ON, Canada), based on an electrodeless

radio-frequency (r.f., 100 MHz)-powered discharge. Depending on the particular

lamp, noble gas such as Krypton (Kr) or Xenon (Xe) is sealed into a high-grade Pyrex

ampoule with a MgF_2 window (cut-off wavelength, λ=112 nm), as described in detail

elsewhere.[23, 27-28] The spectral characteristics of the different VUV sources are

summarized in **Figure 3** and **Table 2**. Compared to the "Resonance" sources, the Hg

lamp shows several emission lines, the most pronounced being at λ=253.7 nm.

However, only the emission at λ=184.9 nm was of importance in this work based on

$k(\lambda)$ of the two precursor gases, and it represents about 7% of the lamps' total output,

$I_{184.9\ nm,\ 5.08\ cm,\ air}$ =177 μW/cm^2. In order to integrate this lamp to the VUV reactor

chamber, it was placed in front of a flanged fused silica window, which assured good
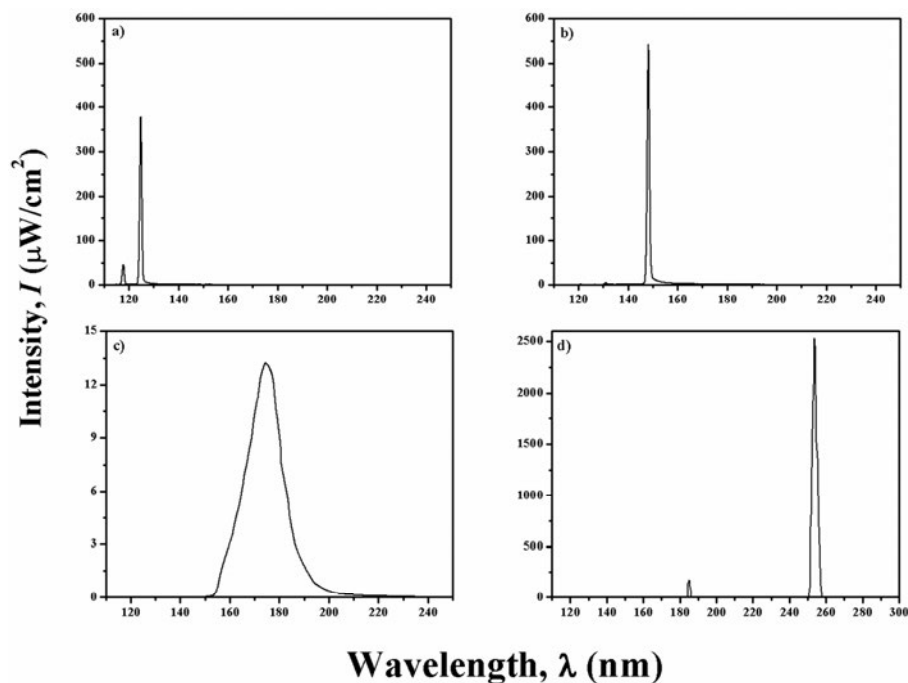
vacuum in the reactor chamber.

12

Figure 3. Intensities and spectral distributions of the VUV radiation emitted by the a) resonant Kr; b) resonant Xe; c) Xe excimer (as measured by Truica et al.[27-28, 32] at d = 6.0 cm under high vacuum); and d) Hg lamps (spectrum obtained from the manufacturer, corresponding to d=5.08 cm[49] in air).

Table 2. Characteristics of the VUV sources used, measured under high vacuum at the respective frontal distances, d (see text).

Lamp	Peak Wavelength, λ_{peak} (nm)	Photon Energy, E_p (eV)	Photon Flux, Φ (ph/cm^2/s)
KrL	123.6	10.0	$1.4 \cdot 10^{15}$
XeL	147.0	8.4	$2.5 \cdot 10^{15}$

13

XeE	172.0	7.2	$6.3 \cdot 10^{14}$
Hg	184.9	6.7	$7.1 \cdot 10^{15}$

The c-Si substrates were mounted on a stainless-steel sample holder, which could be moved axially within the VUV reactor chamber, to frontal distances of d_{KrL}=0.9 cm, d_{XeL}=0.9 cm, and d_{XeE}=0.7 cm. Varying d between the substrate and the VUV source allowed us to vary the photon flux, Φ, impinging on the gas mixture in the gap. In the case of the Hg source, the lamp was moved to d_{Hg}=8.0 cm away from the fused silica window, behind which the c-Si substrate was placed. This allowed us to achieve comparable experimental Φ values (see Table 2) while guaranteeing deposit creation on the c-Si substrates. Earlier work by Truica et al.[27-28, 32] had shown that a $\Phi \sim d^{-2}$ relationship quite closely applied to the "Resonance" lamps at the sample holder/substrate, even though these were far from being "point-sources". To determine Φ, the photocurrent, i, of each source was measured at different d from the respective source under high vacuum inside the chamber, using two NIST-calibrated photodiodes (Resonance Ltd., Barrie, ON, Canada). This allowed us to obtain Φ as a function of d and thus to determine the above-mentioned distances for each source at which comparable photon fluxes would act at the position of the c-Si substrates. Coatings of comparable thicknesses ($\sim$ 50 nm) were obtained by varying the treatment duration between 1 and 5 h (depending on the VUV source and gas mixture ratio).

14

For reasons of safety in handling the toxic H_2S, the experimental chamber was housed inside a N_2-filled glovebox; this had the additional benefit of inhibiting oxygen-exposure and "aging" of the freshly-deposited UV-PA:S films when the chamber was opened.

Characterization studies

X-ray photoelectron spectroscopy

All deposits were characterized by X-ray photoelectron spectroscopy (XPS), performed in a Thermo Scientific K-Alpha[TM] instrument (Waltham, MA, USA) using monochromatic Al Kα radiation (hv=1486.6 eV). The samples were mounted onto a vacuum transfer module (VTM, Thermo Scientific K-Alpha[TM]) inside the glovebox and directly transferred to the instrument without exposure to air; this allowed us to determine the UV-PA:S films' native chemical composition without exposure to atmospheric O_2. The elemental compositions (in atomic %, at. %) and chemical environments of the constituent elements were obtained by survey- and high-resolution (HR) spectra, respectively. The former were acquired at a pass energy of 160 eV, a dwell time of 200 ms and energy steps of 1 eV, the latter at pass energy of 20 eV, dwell time of 200 ms and energy steps of 0.1 eV. No evidence of X-ray induced damage was observed, based on measurements of the C1s peaks before and after analyses. Spectra were acquired at 0° emission angles, and possible charging was corrected by referencing all peaks to the HR C1s peak at binding energy (BE) = 285.0 eV. The constituent elements were quantified from the broad-scan spectra using CasaXPS v2.3.16 (CasaSoftware Ltd., Teignmouth, England), by integrating the areas

15

under relevant peaks after a Shirley-type background subtraction, and by using sensitivity factors from the Wagner table.[50] Throughout this study, we refer to the atomic sulfur concentration, [S], of UV-PA:S coatings; however, since hydrogen atoms cannot be detected by XPS, [S] is approximated by:

$$[S] = \frac{S}{S + O + C} \times 100 \qquad \textbf{(8)}$$

Chemical derivatization with *N*-ethylmaleimide

Chemical derivatization with *N*-ethylmaleimide (98%, BioShop Canada Inc., Burlington, ON, Canada) was used to quantify thiol concentrations, [SH], as recently described by Thiry et al.[51] The reaction mechanism is shown in **Scheme 1**, where *N*-ethylmaleimide reacts selectively with SH via nucleophilic addition between the S atom and the double bond in the maleimide structure (thiol-ene click reaction), forming a stable thio-ether bond. The thiol-maleimide reaction offers several advantages, including high selectivity in the presence of multiple functional groups, rapid and quantitative conversion at low thiol concentrations, and high stability in aqueous environments.[52]
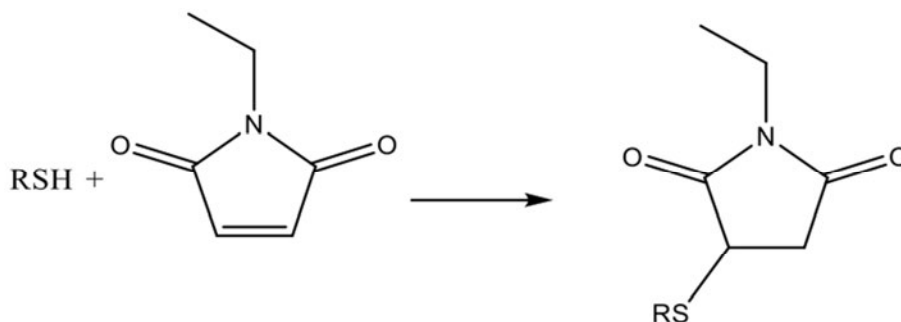
Scheme 1. Derivatization reaction between a thiol group and N-ethylmaleimide.

The derivatization reaction was carried out in phosphate buffer solution (PBS) at pH=7, the *N*-ethylmaleimide concentration being fixed at 0.1 M. Since free thiol functionalities are sensitive towards oxidation upon exposure to oxygen,[14, 53] the samples were mounted into closed vials, equipped with a septum, before removal from the glovebox, thereby eliminating possible exposure to air. The derivatization solution was then injected through the septum and the samples were kept immersed in this solution for 78 h, following which they were rinsed in clean solution for 5 min to eliminate any unreacted molecules, then finally dried under a flow of dry nitrogen. XPS survey spectra were obtained before and after derivatization, allowing nitrogen, [N], and carbon, [C], concentrations to be quantified; [SH], was then calculated as follows:

$$[SH] = \frac{[N]}{[C] - 6[N]} \times 100 \ (\%) \qquad \textbf{(9)}$$

Profilometry

The coating thickness, T, was measured by scratching down to the c-Si substrate using a sharp needle. The resulting step height was measured with a Dektak XTTM Stylus Profilometer (Bruker, Tucson, AZ, USA), using a diamond tip and an applied force of 3 mg. The measured T was used to determine deposition rates, r (nm/min), which in turn were used to determine the normalized deposition rates shown in **Figure 5**, using the respective photon flux of each VUV source listed in **Table 2**.

Atomic Force Microscopy

The surface morphology of the films was investigated by atomic force microscopy (AFM) using a MFP-3D instrument (Asylum Research, Santa Barbara, CA, USA). All samples were measured in tapping mode using silicon cantilevers (ACTA model, AppNano) with a nominal spring constant of 37 N/m, nominal resonant frequency of 300 kHz, and nominal tip radius of 6 nm. Gwyddion 2.48 software was used to process the AFM images.

RESULTS AND DISCUSSION

Deposition kinetics

As explained in the section entitled *Wavelength-dependent photolysis of C_2H_2 and H_2S*, the photo-dissociation and therefore depositon was dependent on $k(\lambda)$ of the individual precursor gases. However, when considering mixtures as in this present study, $k(\lambda)$ must first be used to calculate absorption coefficients of the gas mixtures,

18

α, considering the mixture ratios , $R = \frac{F(H_2S)}{F(C_2H_2)}$, the intensity of the sources, I, and the

pressure, p. Truica et al.[9, 23] reported the following equation to calculate α:

$$\alpha = \int \left(\frac{1}{R+1} k(\lambda)_{C2H2} + \frac{R}{R+1} k(\lambda)_{H2S} \right) \frac{I(\lambda)}{\int I(\lambda)d\lambda} p d\lambda$$

(10)

where $\frac{I(\lambda)}{\int I(\lambda)d\lambda}$ is the relative contribution (in %) of each λ value in the overall

emission spectrum of the respective source, and p the gas pressure (here kept constant

at 400 Pa=3 Torr).

The calculated absorption coefficients of the H$_2$S/C$_2$H$_2$ mixtures, α, as a

function of R are presented in **Figure 4**.
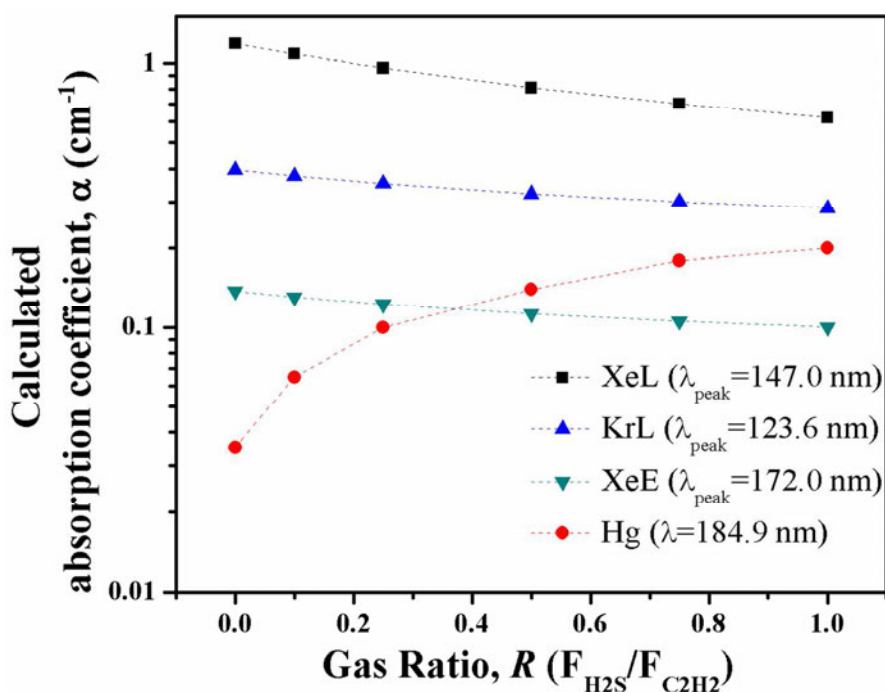
Figure 4. Calculated absorption coefficients, α (in cm^{-1}), calculated using equation

(7) for H_2S/C_2H_2 gas mixtures; the corresponding wavelengths are those of the XeL

(squares), KrL (triangles), XeE (upside down triangles), Hg (circles) VUV sources.

Calculated α values of the H_2S/C_2H_2 mixtures are seen to vary significantly for the

different λ, being highest at λ=147.0 nm, followed by λ=123.6 nm, λ=172.0 nm, and

λ=184.9 nm, respectively. Based on this, one would expect substantial differences in

the photo-induced deposition kinetics at different λ. This was indeed the case, **Figure**

5, where deposition rates normalized with respect to photon flux, r/Φ, are seen to have

followed the same trend as α. The ratio r/Φ is being considered, so as to remove

possible dependence of r on the number of photons, in other words, focusing only on
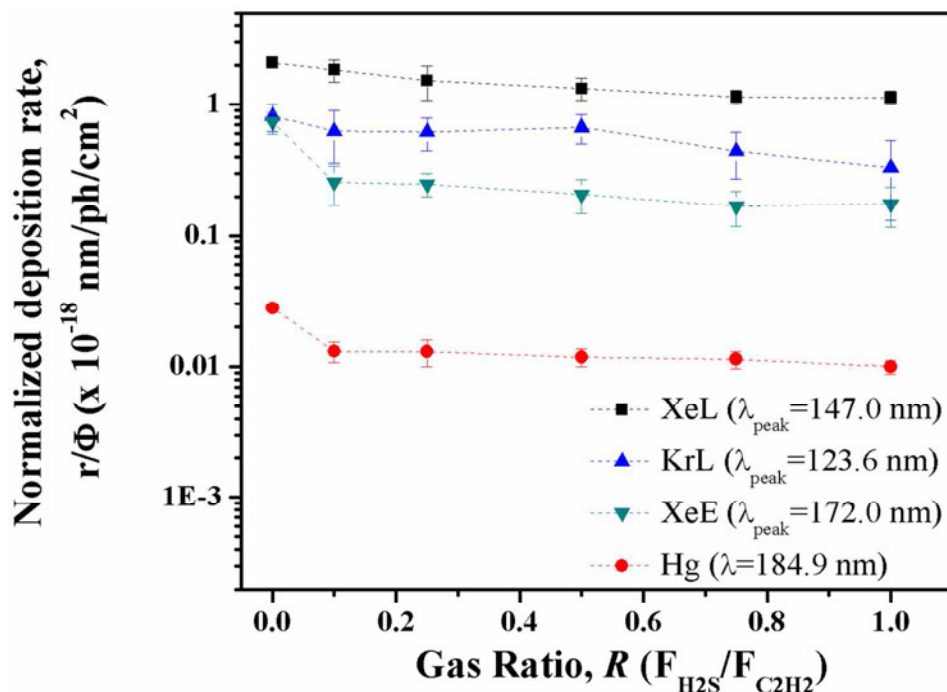
the λ–dependence.

20

Figure 5. Normalized deposition rates, r/Φ, as a function of gas mixture ratio, R, for UV-PA:S films deposited using the XeL (squares), KrL (triangles), XeE (upside down triangles), Hg (circles) sources. Error bars indicate 95% confidence interval. The lines are to guide the reader's eye.

Overall, r/Φ values are seen to have decreased with rising R, for XeL from 2.1 ($R=0$) to 1.1×10^{-18} nm/ph/cm^2 ($R=1$); from 0.8 to 0.3 $\times 10^{-18}$ nm/ph/cm^2 for KrL; from 0.7 to 0.2 $\times 10^{-18}$ nm/ph/cm^2 for XeE; and from 0.03 to 0.01 $\times 10^{-18}$ nm/ph/cm^2 for Hg. This comes as no surprise, since, except for Hg, all α values decreased with rising R. For Hg, an increase in α was due to higher k of H_2S at $\lambda=184.9$ nm. The overall rate at which precursor radicals were produced decreased with increasing R, which also reduced the relative concentration of $C_xH_y\cdot$ radicals, and thereby also the formation of UV-PA:S.[9, 23, 27] Furthermore, increasing R also gave rise to a greater concentration

21

of reactive H atoms, leading to competing etching reactions, hence to the decrease in

r/Φ for all four VUV sources.[9, 22]

It is noteworthy that pure acetylene-based, amorphous carbon films (R=0) had

been obtained in the past through PICVD by Danno et al.[54] using a low-pressure Hg

lamp. The carbon films were deposited at elevated temperatures (150 and 300°C),

under conditions resulting in r/Φ values of $1.8\mathrm{x}10^{-17}$ nm/ph/cm^2 and $7.2\mathrm{x}10^{-18}$

nm/ph/cm^2, respectively, compared to $3\mathrm{x}10^{-20}$ nm/ph/cm^2 in the present work (at

room temperature). Differences between setup geometries and process parameters

(even though Danno also used p=400 Pa=3 Torr) could help explain the higher

deposition rates obtained by the Japanese authors.

Chemical composition of deposited UV-PA:S films

Chemical compositions, more particularly [S] as a function of R, are seen to have

displayed different trends among the four different UV-PA:S film families (**Figure 6**).

An example of an XPS survey spectrum, which was used to obtain [S], is

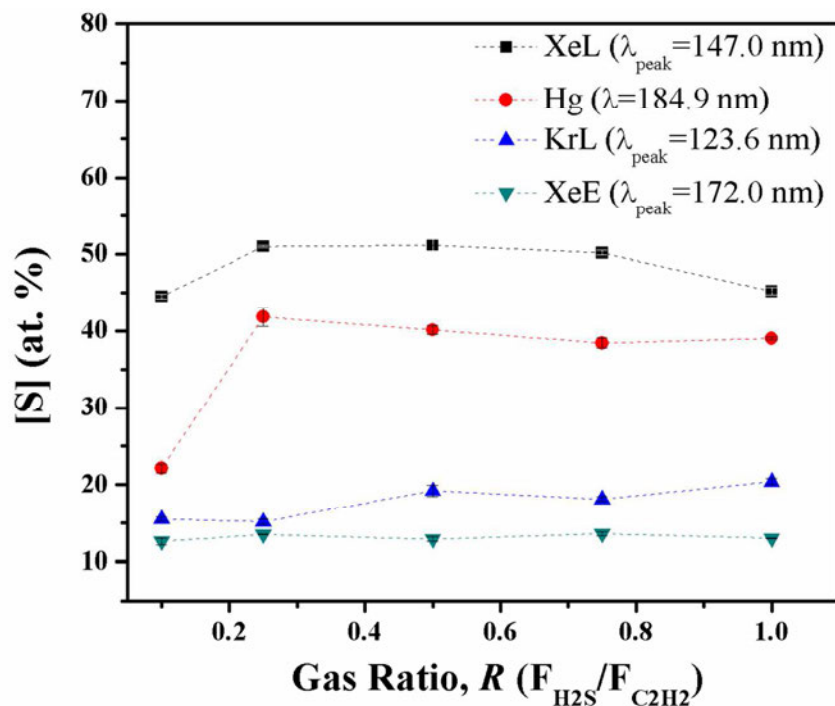demonstrated in **Figure S1** in the Supporting Information.

22

Figure 6. Sulfur concentrations, [S] (in at.- %) of UV-PA:S films deposited using XeL (squares), KrL (triangles), XeE (upside down triangles), Hg (circles) VUV sources, as a function of gas mixture ratio, R. The lines are to guide the reader's eye.

On the basis of **Figure 1** and **Table 1**, the highest $k(\lambda)$ values of H_2S at $\lambda=184.9$ nm might lead one to expect the highest [S] for the case of the Hg VUV lamp, but the most efficient S-incorporation in fact was observed for XeL. In order to incorporate S-containing groups into UV-PA:S, the polymer-like backbone needs to be created first and foremost. For the case of XeL the probability of $C_xH_y\cdot$ radical creation by photo-dissociation of C_2H_2 was obviously high, thereby possibly also allowing higher incorporation of S. However, for the case of the Hg source, the rate of creating $C_xH_y\cdot$ radicals was much smaller, even though the possibility of S incorporation was higher Tentatively, this would explain why [S] ~ 50 and ~ 40 at.% for the XeL and Hg

lamps, respectively, as observed in **Figure 6**. In terms of possible reaction mechanisms, if only "pure" thiol-yne chain reactions (**(6)** and **(7)**) would take place, a film composition of $(SCH_2CH_2)_n$, resulting in [S]=33 at.% could be expected. However, since [S]>33 at. % (in the case of the Hg and XeL sources), we can assume that this is not the only formation mechanism. Many subsequent reactions are possible, resulting in a broad product distribution. Contrary to trends of increasing heteroatom concentration (here: S) with rising R values reported in the literature and in our previous work,[9, 22, 55] **Figure 6** did not bear witness to such an increase in [S]. Here, [S] of the UV-PA:S films tended to rise between R=0.1 and 0.25, but it then remained nearly constant when R further increased. We attribute this to the higher pressure (p=400 Pa=3 Torr) used in the present experiments, compared to p « 133 Pa=1 Torr in previous studies. In an attempt to better understand this rather unusual behavior noted in **Figure 6**, UV-PA:S films were deposited at p=13 Pa=0.1 and 133 Pa=1 Torr using only the KrL and XeL VUV sources (**Figure 7**). Only these two yielded sufficiently high r values at the lower p, due to the dependence of quantum yield on p discussed in the earlier section entitled *Wavelength-dependent photolysis of C_2H_2 and H_2S.*
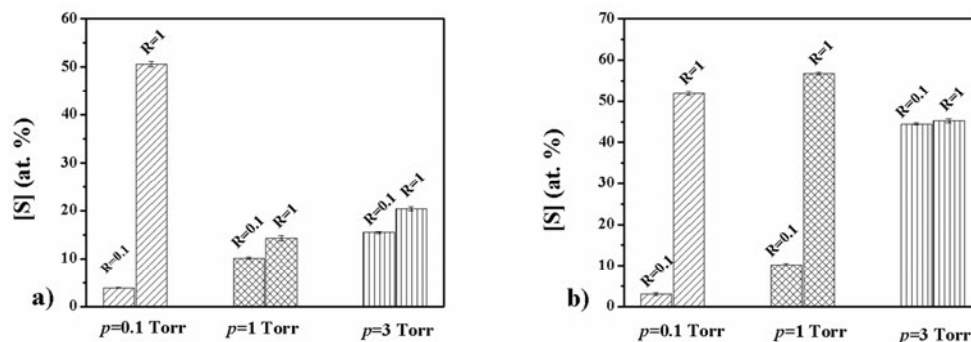
24

Figure 7. Sulfur concentrations, [S] (in at.- %), for UV-PA:S films deposited using the a) KrL and b) XeL VUV sources at three different pressures (p=13, 133, and 400 Pa=0.1, 1 and 3 Torr) and two gas mixture ratios (R=0.1 and 1).

At low p (p=13 Pa=0.1 Torr), a dramatic increase in [S] with rising R was observed, as also reported in the literature and in our own previous work. As p increased, numbers of molecular collisions of course also increased, leading to more S-bearing reactive species and more sulfur incorporation into the films. In **Figure 7**, [S] values at R=1 and lower p were seen to significantly exceed those at higher p, especially for XeL radiation, while at p=400 Pa=3 Torr [S] values were almost independent of R, as observed in **Figure 6**.

Changing p could also lead to transitions among different flow regimes, of which one can distinguish three, depending on p and on geometry: these are molecular, continuum and transition flows. They can be quantitatively distinguished by their respective dimensionless Knudsen numbers, K_n:

$$K_n = \frac{l}{d}$$

(11)

where l is the molecular mean free path and d a characteristic length of the experimental apparatus; in this case we chose d to be the distance between lamp and substrate where deposition occurred. Mean free path, l, the average distance between collisions among gas molecules, is given by[56-57]

$$l = \frac{k_B T}{\sqrt{2}\sigma p} = \frac{k_B T}{\sqrt{2}\pi \left(\frac{1}{2}d_1 + \frac{1}{2}d_2\right)^2 p_1 p_2} \qquad \textbf{(12)}$$

for the case of gas mixtures with dissimilar particles. In equation **(12)**, k_B is Boltzmann's constant, T the temperature, σ the collisional cross-section, and p the pressure. To consider collisions between the dissimilar particles here, the molecular diameters of H_2S (d_1=3.6·10^{-10} m) and of C_2H_2 (d_2=3.3·10^{-10} m), and their partial pressures (p_1 and p_2) need to be considered. Knudsen numbers, $K_n < 0.01$ describe continuum flow, whereas $K_n > 1$ represent molecular or discrete particle flow. Between those values both gas-gas and gas-wall collisions are important, and the flow regime is termed transition or slip flow.[56-58] Here, the two mixture ratios (R=0.1 and 1) and three different pressures (p=13, 133 and 400 Pa=0.1, 1 and 3 Torr) yielded $K_n \sim 0.1$ at p=13 Pa=0.1 Torr; ~0.001 at p=133 Pa=1 Torr; and ~5·10^{-5} at p=400 Pa=3 Torr (*see Supporting Information for detailed calculations*). Therefore, we have observed a shift between transition and continuum flow regimes. As p increased and transition towards continuum flow occurred, collisions gained in importance, transition towards continuum flow being observed between p=13 and 133 Pa (=0.1 and 1 Torr) (K_n<<0.01). We propose that this transition may explain the different [S] versus R behaviours observed in **Figure 6** and **Figure 7**. Such a dependence of chemical

26

composition on p is an important observation, one which to the authors' knowledge has so far not yet been reported in connection with transitions among flow regimes. This aspect of very different heteroatom incorporation rates may well need to be taken into consideration when in future designing new CVD processes.

Because [S] does not reveal in what functional form this element was incorporated in the UV-PA:S films, the selective and quantitative derivatization reaction based on N-ethylmaleimide was used to determin [SH], as shown in **Figure 8**. A typical XPS survey spectrum obtained after the derivatization reaction is shown in Figure S1 in the Supporting Information.
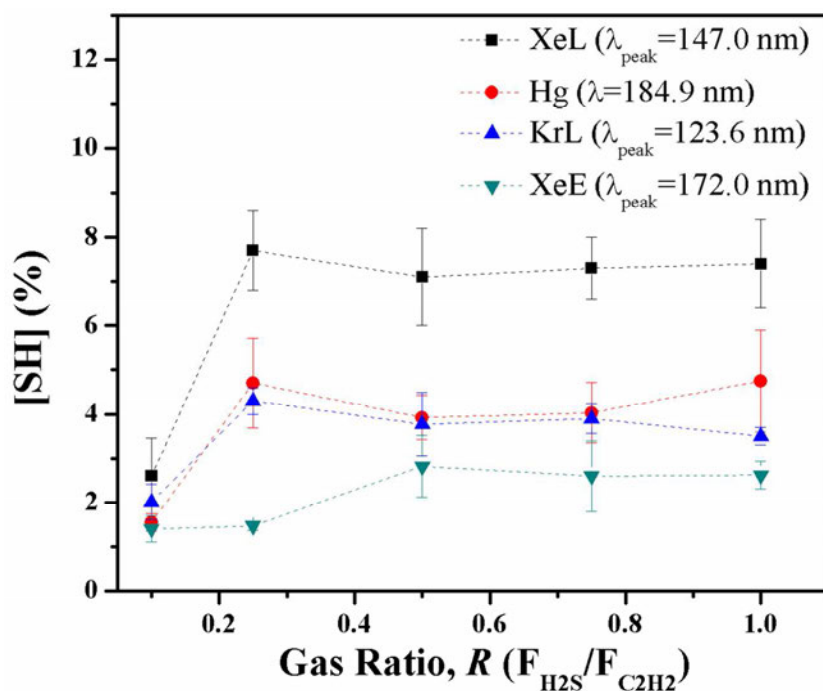

Figure 8. Proportion of C bearing -SH groups, [SH] (in %), determined using chemical derivatization XPS for UV-PA:S films based on XeL (squares), KrL (triangles), XeE (upside down triangles), Hg (circles) VUV sources, versus   gas

27

mixture ratio, R. Error bars show standard deviations of three measurements. The lines are to guide the reader's eye.

This plot of [SH] versus R displays similar trends as that of [S] versus R in **Figure 6**, the highest incorporation of thiol groups having occurred for the case of XeL-based deposits, followed by Hg, KrL and XeE ones. Following an initial increase in [SH] between R=0.1 and 0.25, [SH] values are seen to have remained nearly constant. These UV-PA:S films, especially in the case of XeL, were much richer in SH groups than their L-PPA:S ("low-pressure plasma-polymerized, sulfurized acetylene") counterparts, reported in our previous study;[22] here, [SH] values up to ~7.7 % were achieved by photo-polymerization, in sharp contrast with the maximum of only ~3.4 % for L-PPA:S. This was not only the case for the present gas mixtures, but also for a single molecule precursor, propanethiol, where a maximum [SH] of ~5 % was obtained.[51] It is noteworthy that comparable [SH] (~5 %) was achieved using the Hg lamp, far more affordable and readily available than the other three VUV sources used here.

The observed higher photochemical [SH] values for UV-PA:S films compared with their plasma-chemical L-PPA:S counterparts is not entirely surprising, because this has already been observed and reported for N- and O-rich films.[9, 23] Indeed, Truica reported UV-PE:N deposits with up to more than 70 % [-NH$_2$] concentration (versus roughly 30 % for L-PPE:N) when using C_2H_4-NH_3 reagent gas mixtures. In low-pressure plasma, the gaseous precursors are subjected to many collisions with "hot" electrons that possess Boltzmann-like energy distribution. However, as stated

28

earlier, photolysis of H_2S creates only SH· radicals, which react with hydrocarbon radicals under much lesser disruption than in a discharge plasma. For this reason [SH] values for the XeL-based UV-PA:S were the highest ones reported in the literature so far for any preparation method or type of precursor. They greatly exceeded ones previously reported (up to ~1.75 %),[22] where photo-polymerized S-containing films were prepareded using mixtures of C_2H_4 or butadiene (C_4H_6) with H_2S using the KrL source. Beside the selective and specific VUV-photochemical reactions via the present gas mixtures, a further reason for the high [SH] can be attributed to the exclusion of oxygen during derivatization, i.e. no oxidation of free thiol groups. To the authors' best knowledge such air-excluding derivatization had not been reporteded before, but it can evidently have contributed significantly to increased retention of SH-groups.

While stability studies were beyond the scope of the present work, previous studies suggest that these photo-derived films should be stable in aqueous media, suitable for further applications.[9, 22, 59]

Surface morphology

Growth mechanisms and resulting surface-topological features are also known to affect the performance of thin coatings for biomaterial uses.[60-61] In designing new biomaterials, it is critically important to consider how cells respond to specific surface-chemical and -topographical features. Therefore, we have examined the

29

surface morphologies of UV-PA:S films deposited using the four different VUV sources at R=0.1 and R=1, see **Figure 9**.
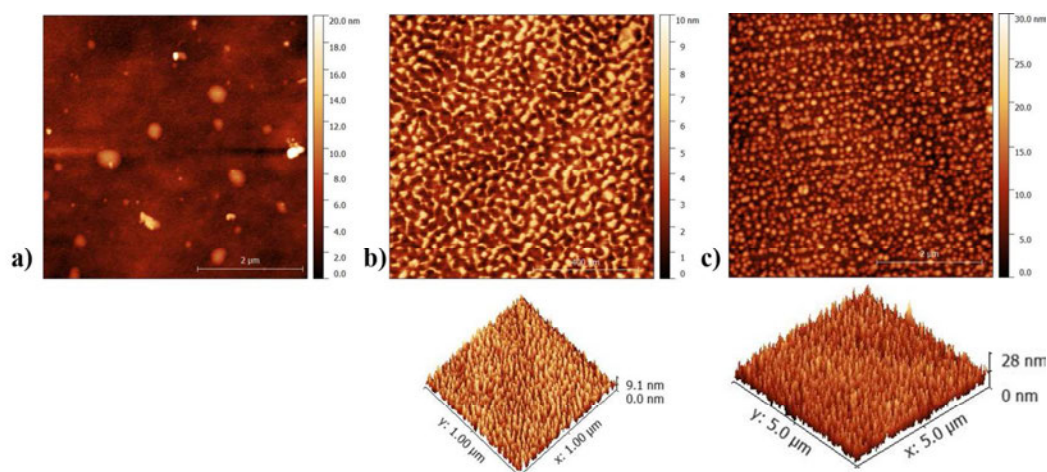
Figure 9. Atomic force microscopy topography images of UV-PA:S films deposited using the KrL VUV source at a) R=0.1 (5x5 μm^2); b) R=0.1 (1x1 μm^2); and (c) R=1 (1x1 μm^2). The bottom images represent 3D portrayals of the respective surfaces.

At lower magnification (5x5 μm^2, **Figure 9 a)**), the R=0.1 film appeared smooth , but at higher magnification (i.e. smaller area, 1x1 μm^2) the AFM images reveal a rougher surface with island-like features up to ~4 nm in height (**Figure 9 b)**). These were more pronounced at R=1 and were seen to grow in height up to ~14 nm (**Figure 9 c)**): The films' RMS roughness increased with rising R, from ~1.5 nm to ca. 5.4 nm. Similar island-like features with increasing R were also observed for the other VUV sources. For example, **Figure 10** represents UV-PA:S films obtained with the Hg source, from which we conclude that surface morphology of UV-PA:S was essentially independent of λ, but that it was strongly influenced by R.
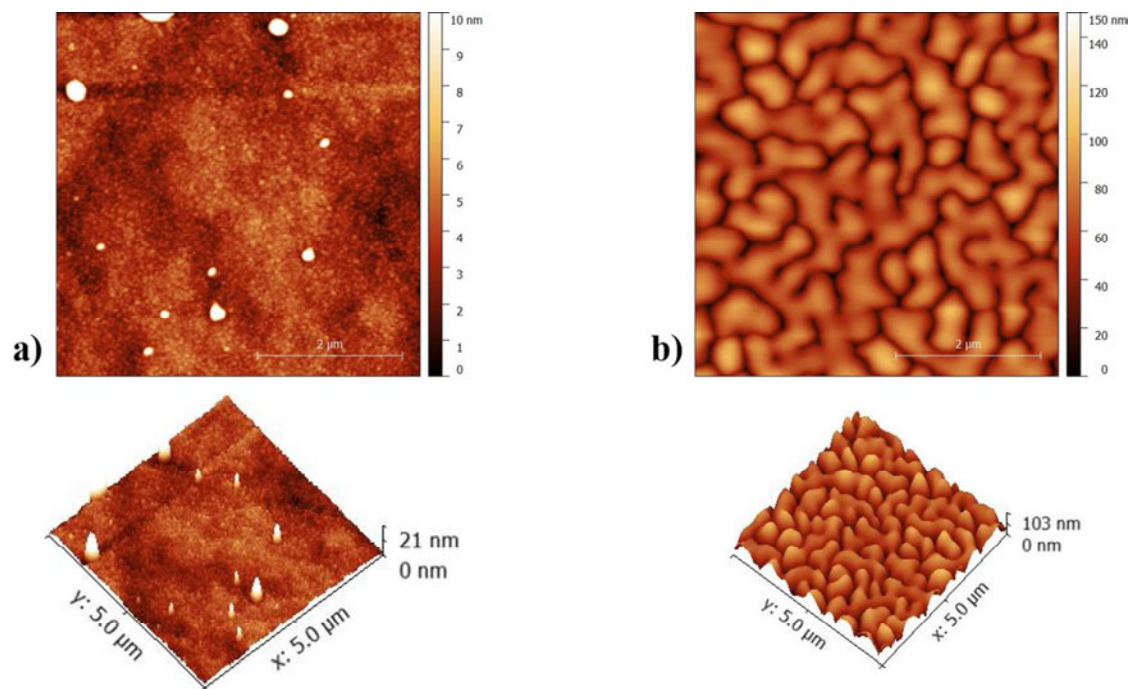
30

Figure 10. Atomic force microscopy topography images of UV-PA:S films deposited using the Hg VUV source at a) R=0.1 (5x5 µm^2); and b) R=1 (5x5 µm^2). The bottom images represent 3D portrayals of the respective surfaces.

Plasma polymers with diverse surface topographies are well known in the literature.[61-64] UV-PA:S appears to present Volmer-Weber growth morphology, where incoming film-forming precursors have more affinity for one another than for the (c-Si) substrate surface. As a result, they tend to form clusters which grow into 3D islands that can eventually coalesce and merge into a continuous film.[60, 63, 65] In terms of surface energy, γ, the deposit tends to form islands minimizing its surface, if its γ is significantly different from that of the underlying substrate, since no intermolecular interactions with the substrate occur. From this, we could infer that the surface energy of the UV-PA:S films deviates from γ of the substrate with rising R and thus with [S].

31

SUMMARY AND CONCLUSIONS

PICVD techniques have been gaining interest over the past years, for example for selective, specific organic surface functionalization. Simply by selecting different photon energies (i.e. values of λ), thin films with different properties could be obtained in this present work. Although different VUV photon energies could be useful in surface engineering, very few wavelength (λ)-dependent deposition studies had been carried out so far. The present study aimed to understand λ-dependent deposition of thiol-terminated films using four different VUV sources covering roughly 123 nm $\leq \lambda \leq$ 185 nm. We have shown that UV-PA:S coatings could be successfully deposited by VUV irradiation of acetylene (C_2H_2) / hydrogen sulfide (H_2S) mixtures, growth rates and properties of the resulting films being highly λ-dependent. The results clearly showed that photolytic reactions of C_2H_2 and H_2S are governed by the gases' absorption coefficients, $k(\lambda)$, obviously also that of the H_2S/C_2H_2 gas mixtures, α. The latter was found to be highest for the XeL VUV source, and was found to yield the highest sulfur, [S], and thiol, [SH], concentrations. [SH] values reported here are the highest in the literature so far, a good choice if high [SH] are desired for further (biomedical) applications. Slightly lower [SH] ($\sim$5%) were obtained with the more economic and readily accessible Hg lamp. The importance of pressure, p, another key CVD process parameter was also amply demonstrated in the section entitled *Wavelength-dependent photolysis of C_2H_2 and H_2S*. This was especially evident from the [S] versus R dependence: surprisingly, at the relatively high p=400 Pa=3 Torr, used here, [S] remained nearly constant with R

32

contrary to all previous studies by others and by ourselves.[9, 22, 55, 66] Independent of

λ, UV-PA:S deposits showed island-like growth morphology, more pronounced with

increasing [S].

In summary, this λ-dependent VUV photo-deposition study demonstrated the

importance of single, well-characterized VUV sources for selective and specific

deposition of organic coatings. This UV-PA:S deposition technique can be useful for

creating optimized films with desired biomedical properties simply by adjusting the

source's wavelength.

ASSOCIATED CONTENT

Supporting Information

XPS survey spectra of typical UV-PA:S film before and after derivatization

Detailed calculation of the Knudsen number

AUTHOR INFORMATION

Corresponding Author

*Email: pierre-luc.girard-lauriault@mcgill.ca

ORCIC

Evelyne Kasparek: 0000-0002-9406-5627

Jason R. Tavares: 0000-0002-3828-2993

33

REFERENCES

1.   Ikada, Y., Surface modification of polymers for medical applications. *Biomaterials* **1994,** *15* (10), 725-736.
2.   Goddard, J. M.; Hotchkiss, J., Polymer surface modification for the attachment of bioactive compounds. *Progress in polymer science* **2007,** *32* (7), 698-725.
3.   Chu, P. K.; Chen, J.; Wang, L.; Huang, N., Plasma-surface modification of biomaterials. *Materials Science and Engineering: R: Reports* **2002,** *36* (5), 143-206.
4.   Liston, E.; Martinu, L.; Wertheimer, M., Plasma surface modification of polymers for improved adhesion: a critical review. *Journal of adhesion science and technology* **1993,** *7* (10), 1091-1127.
5.   Tavares, J.; Shahryari, A.; Harvey, J.; Coulombe, S.; Omanovic, S., Corrosion behavior and fibrinogen adsorptive interaction of SS316L surfaces covered with ethylene glycol plasma polymer-coated Ti nanoparticles. *Surface and Coatings Technology* **2009,** *203* (16), 2278-2287.
6.   Siow, K. S.; Britcher, L.; Kumar, S.; Griesser, H. J., Plasma methods for the generation of chemically reactive surfaces for biomolecule immobilization and cell colonization-a review. *Plasma processes and polymers* **2006,** *3* (6-7), 392-418.
7.   Förch, R.; Chifen, A. N.; Bousquet, A.; Khor, H. L.; Jungblut, M.; Chu, L. Q.; Zhang, Z.; Osey-Mensah, I.; Sinner, E. K.; Knoll, W., Recent and expected roles of plasma-polymerized films for biomedical applications. *Chemical Vapor Deposition* **2007,** *13* (6-7), 280-294.
8.   Girard-Lauriault, P. L.; Mwale, F.; Iordanova, M.; Demers, C.; Desjardins, P.; Wertheimer, M. R., Atmospheric pressure deposition of micropatterned nitrogen-rich plasma-polymer films for tissue engineering. *Plasma Processes and Polymers* **2005,** *2* (3), 263-270.
9.   Truica-Marasescu, F.; Ruiz, J. C.; Wertheimer, M. R., Vacuum-ultraviolet (VUV) Photo-polymerization of Amine-rich Thin Films from Ammonia–Hydrocarbon Gas Mixtures. *Plasma Processes and Polymers* **2012,** *9* (5), 473-484.
10.   Harris, J. M., *Poly (ethylene glycol) chemistry: biotechnical and biomedical applications*. Springer Science & Business Media: 2013.
11.   Ravi, S.; Krishnamurthy, V. R.; Caves, J. M.; Haller, C. A.; Chaikof, E. L., Maleimide–thiol coupling of a bioactive peptide to an elastin-like protein polymer. *Acta biomaterialia* **2012,** *8* (2), 627-635.
12.   Ghosh, S. S.; Kao, P. M.; McCue, A. W.; Chappelle, H. L., Use of maleimide-thiol coupling chemistry for efficient syntheses of oligonucleotide-enzyme conjugate hybridization probes. *Bioconjugate chemistry* **1990,** *1* (1), 71-76.
13.   Tsai, Y.-T.; Wu, C.-Y.; Guan, Z.-Y.; Sun, H.-Y.; Cheng, N.-C.; Yeh, S.-Y.; Chen, H.-Y., Topologically Controlled Cell Differentiation Based on Vapor-Deposited Polymer Coatings. *Langmuir* **2017,** *33* (36), 8943-8949.

34

14.   Nimmo, C. M.; Shoichet, M. S., Regenerative biomaterials that "click": simple, aqueous-based protocols for hydrogel synthesis, surface immobilization, and 3D patterning. *Bioconjugate chemistry* **2011,** *22* (11), 2199-2209.

15.   Jonkheijm, P.; Weinrich, D.; Köhn, M.; Engelkamp, H.; Christianen, P.; Kuhlmann, J.; Maan, J. C.; Nüsse, D.; Schroeder, H.; Wacker, R., Photochemical Surface Patterning by the Thiol-Ene Reaction. *Angewandte Chemie* **2008,** *120* (23), 4493-4496.

16.   Weinrich, D.; Lin, P. C.; Jonkheijm, P.; Nguyen, U. T.; Schröder, H.; Niemeyer, C. M.; Alexandrov, K.; Goody, R.; Waldmann, H., Oriented Immobilization of Farnesylated Proteins by the Thiol-Ene Reaction. *Angewandte Chemie International Edition* **2010,** *49* (7), 1252-1257.

17.   Harris, L.; Schofield, W.; Doores, K.; Davis, B.; Badyal, J., Rewritable glycochips. *Journal of the American Chemical Society* **2009,** *131* (22), 7755-7761.

18.   Schofield, W.; McGettrick, J.; Bradley, T.; Badyal, J.; Przyborski, S., Rewritable DNA microarrays. *Journal of the American Chemical Society* **2006,** *128* (7), 2280-2285.

19.   Aparicio, F. J.; Thiry, D.; Laha, P.; Snyders, R., Wide Range Control of the Chemical Composition and Optical Properties of Propanethiol Plasma Polymer Films by Regulating the Deposition Temperature. *Plasma Processes and Polymers* **2016,** *13* (8), 814-822.

20.   Thiry, D.; Britun, N.; Konstantinidis, S.; Dauchot, J.-P.; Denis, L.; Snyders, R., Altering the sulfur content in the propanethiol plasma polymers using the capacitive-to-inductive mode transition in inductively coupled plasma discharge. *Applied Physics Letters* **2012,** *100* (7), 071604.

21.   Thiry, D.; Francq, R.; Cossement, D.; Guillaume, M.; Cornil, J.; Snyders, R., A detailed description of the chemistry of thiol supporting plasma polymer films. *Plasma Processes and Polymers* **2014,** *11* (6), 606-615.

22.   Kasparek, E.; Tavares, J. R.; Wertheimer, M. R.; Girard-Lauriault, P. L., Sulfur-Rich Organic Films Deposited by Plasma-and Vacuum-Ultraviolet (VUV) Photo-Polymerization. *Plasma Processes and Polymers* **2016,** *13* (9), 888-899.

23.   Truica-Marasescu, F.; Wertheimer, M. R., Vacuum-Ultraviolet Photopolymerisation of Amine-Rich Thin Films. *Macromolecular Chemistry and Physics* **2008,** *209* (10), 1043-1049.

24.   Dorval Dion, C. A.; Raphael, W.; Tong, E.; Tavares, J. R., Photo-initiated chemical vapor deposition of thin films using syngas for the functionalization of surfaces at room temperature and near-atmospheric pressure. *Surface and Coatings Technology* **2014,** *244*, 98-108.

25.   Farhanian, D.; De Crescenzo, G.; Tavares, J. R., Kinetics, Chemistry, and Morphology of Syngas Photoinitiated Chemical Vapor Deposition. *Langmuir* **2017,** *33* (8), 1780-1791.

26.   Hanabusa, M., Photoinduced deposition of thin films. *Materials Science Reports* **1987,** *2* (2), 51-97.

27.   Truica-Marasescu, F.; Pham, S.; Wertheimer, M. R., VUV processing of polymers: Surface modification and deposition of organic thin films. *Nuclear Instruments and Methods in Physics Research Section B: Beam Interactions with Materials and Atoms* **2007,** *265* (1), 31-36.

28.   Truica-Marasescu, F.; Wertheimer, M., Vacuum ultraviolet–induced photochemical nitriding of polyolefin surfaces. *Journal of applied polymer science* **2004,** *91* (6), 3886-3898.

29.   Dion, C. D.; Tavares, J. R., Photo-initiated chemical vapor deposition as a scalable particle functionalization technology (a practical review). *Powder technology* **2013,** *239*, 484-491.

30.   Armstrong, J. V.; Burk, A. A.; Coey, J. M. D.; Moorjani, K., Wavelength control of iron/nickel composition in laser induced chemical vapor deposited films. *Appl. Phys. Lett. Applied Physics Letters* **1987,** *50* (18), 1231-1233.

31.   Hanabusa, M.; Ikeda, M., Wavelength dependence in photochemical vapor deposition of aluminum film using dimethylaluminum hydride. *AOC Applied Organometallic Chemistry* **1991,** *5* (4), 289-293.

32.   Truica-Marasescu, F.-E.; Wertheimer, M. R., Vacuum Ultraviolet Photolysis of Hydrocarbon Polymers. *Macromolecular Chemistry and Physics* **2005,** *206* (7), 744-757.

33.   Wu, C. Y. R.; Chen, F. Z.; Judge, D. L., Measurements of temperature-dependent absorption cross sections of C2H2 in the VUV-UV region. *Journal of Geophysical Research-Planets* **2001,** *106* (E4), 7629-7636.

34.   Okabe, H., *Photochemistry of small molecules*. Wiley New York: 1978; Vol. 431.

35.   Stief, L. J.; Decarlo, V. J.; Mataloni, R. J., VACUUM-ULTRAVIOLET PHOTOLYSIS OF ACETYLENE. *J. Chem. Phys.* **1965,** *42* (9), 3113-&.

36.   Laufer, A. H.; Bass, A. M., PHOTOCHEMISTRY OF ACETYLENE - BIMOLECULAR RATE CONSTANT FOR THE FORMATION OF BUTADIYNE AND REACTIONS OF ETHYNYL RADICALS. *Journal of Physical Chemistry* **1979,** *83* (3), 310-313.

35

37.	Lichten, W., Some New Metastable States of Molecules. *The Journal of Chemical Physics* **1962,** *37* (9), 2152-2154.

38.	Zelikoff, M.; Aschenbrand, L. M., VACUUM ULTRAVIOLET PHOTOCHEMISTRY .3. ACETYLENE AT 1849-A. *J. Chem. Phys.* **1956,** *24* (5), 1034-1037.

39.	Irion, M.; Kompa, K., UV laser photochemistry of acetylene at 193 nm. *Applied Physics B* **1982,** *27* (4), 183-186.

40.	Okabe, H., PHOTOCHEMISTRY OF ACETYLENE. *Can. J. Chem.-Rev. Can. Chim.* **1983,** *61* (5), 850-855.

41.	Okabe, H., PHOTOCHEMISTRY OF ACETYLENE AT 1470 A. *J. Chem. Phys.* **1981,** *75* (6), 2772-2778.

42.	Okabe, H., *Photochemistry of small molecules*. Wiley: New York, 1978.

43.	Okabe, H., PHOTOCHEMISTRY OF ACETYLENE AT 1849-A. *J. Chem. Phys.* **1983,** *78* (3), 1312-1317.

44.	Xu, J.; Li, C.; Liu, P.; He, D.; Wang, J.; Zhang, Q., Photolysis of low concentration H2S under UV/VUV irradiation emitted from high frequency discharge electrodeless lamps. *Chemosphere* **2014,** *109* (Supplement C), 202-207.

45.	Darwent, B. d.; Wadlinger, R. L.; Allard, M. J., The photochemical decomposition of hydrogen sulfide. The reactions of hydrogen atoms and HS radicals. *The Journal of Physical Chemistry* **1967,** *71* (7), 2346-2347.

46.	Benedikt, J., Plasma-chemical reactions: low pressure acetylene plasmas. *Journal of Physics D: Applied Physics* **2010,** *43* (4), 043001.

47.	Nobre, M.; Fernandes, A.; da Silva, F. F.; Antunes, R.; Almeida, D.; Kokhan, V.; Hoffmann, S. V.; Mason, N.; Eden, S.; Limao-Vieira, P., The VUV electronic spectroscopy of acetone studied by synchrotron radiation. *Physical Chemistry Chemical Physics* **2008,** *10* (4), 550-560.

48.	Yong, Chun Q.; Jongryang Joo; Donggeun Jung, Polymer-like Organic Thin Films Deposited by Plasma Enhanced Chemical Vapor Deposition Using the Para-xylene Precursor as Low Dielectric Constant Interlayer Dielectrics for Multilevel Metallization. *Japanese Journal of Applied Physics* **1999,** *38* (3R), 1356.

49.	Corporation, A. U. STER-L-RAY Germicidal Ultraviolet Lamps. https://d163axztg8am2h.cloudfront.net/static/doc/7e/4c/84c923fee3d73f7ddbc95af748d6.pdf.

50.	Wagner, C. D.; Davis, L. E.; Zeller, M. V.; Taylor, J. A.; Raymond, R. H.; Gale, L. H., Empirical atomic sensitivity factors for quantitative analysis by electron spectroscopy for chemical analysis. *Surface and Interface Analysis* **1981,** *3* (5), 211-225.

51.	Thiry, D.; Francq, R.; Cossement, D.; Guerin, D.; Vuillaume, D.; Snyders, R., Establishment of a derivatization method to quantify thiol function in sulfur-containing plasma polymer films. *Langmuir* **2013,** *29* (43), 13183-13189.

52.	Xi, W.; Scott, T. F.; Kloxin, C. J.; Bowman, C. N., Click chemistry in materials science. *Advanced Functional Materials* **2014,** *24* (18), 2572-2590.

53.	Van Dijk, M.; Rijkers, D. T.; Liskamp, R. M.; van Nostrum, C. F.; Hennink, W. E., Synthesis and applications of biomedical and pharmaceutical polymers via click chemistry methodologies. *Bioconjugate chemistry* **2009,** *20* (11), 2001-2016.

54.	Danno, M.; Hanabusa, M., AMORPHOUS-CARBON FILMS PREPARED BY PHOTO-CVD FROM ACETYLENE. *Materials Letters* **1986,** *4* (5-7), 261-264.

55.	Contreras-García, A.; Wertheimer, M. R., Low-pressure plasma polymerization of acetylene–ammonia mixtures for biomedical applications. *Plasma Chemistry and Plasma Processing* **2013,** *33* (1), 147-163.

56.	Halwidl, D., *Development of an effusive molecular beam apparatus*. Springer: 2016.

57.	Sivaram, S., *Chemical vapor deposition: thermal and plasma deposition of electronic materials*. Springer Science & Business Media: 2013.

58.	Matteucci, S.; Yampolskii, Y.; Freeman, B. D.; Pinnau, I., Transport of gases and vapors in glassy and rubbery polymers. *Materials science of membranes for gas and vapor separation* **2006,** *1*, 1-2.

59.	Kasparek, E.; Thiry, D.; Tavares, J. R.; Wertheimer, M. R.; Snyders, R.; Girard-Lauriault, P. L., Growth mechanisms of sulfur-rich plasma polymers: Binary gas mixtures versus single precursor. *Plasma Processes and Polymers* **2018**, 1800036.

60.	Michelmore, A., Thin film growth on biomaterial surfaces. *Thin Film Coatings for Biomaterials and Biomedical Applications* **2016**, 29.

61.	Gristina, R.; D'Aloia, E.; Senesi, G. S.; Milella, A.; Nardulli, M.; Sardella, E.; Favia, P.; d'Agostino, R., Increasing cell adhesion on plasma deposited fluorocarbon coatings by changing the

36

surface topography. *Journal of Biomedical Materials Research Part B: Applied Biomaterials* **2009,** *88* (1), 139-149.

62.   Hwang, S.; Seo, H.; Jeong, D. C.; Wen, L.; Han, J. G.; Song, C.; Kim, Y., Growth kinetics of plasma-polymerized films. *Scientific Reports* **2015,** *5*, 5.

63.   Michelmore, A.; Martinek, P.; Sah, V.; Short, R. D.; Vasilev, K., Surface Morphology in the Early Stages of Plasma Polymer Film Growth from Amine-Containing Monomers. *Plasma Processes and Polymers* **2011,** *8* (5), 367-372.

64.   Kylian, O.; Choukourov, A.; Biederman, H., Nanostructured plasma polymers. *Thin Solid Films* **2013,** *548*, 1-17.

65.   Grimoldi, E.; Zanini, S.; Siliprandi, R. A.; Riccardi, C., AFM and contact angle investigation of growth and structure of pp-HMDSO thin films. *The European Physical Journal D* **2009,** *54* (2), 165-172.

66.   Ruiz, J.-C.; Girard-Lauriault, P.-L.; Truica-Marasescu, F.; Wertheimer, M. R., Plasma-and vacuum-ultraviolet (VUV) photo-polymerisation of N-and O-rich thin films. *Radiation Physics and Chemistry* **2010,** *79* (3), 310-314.

37
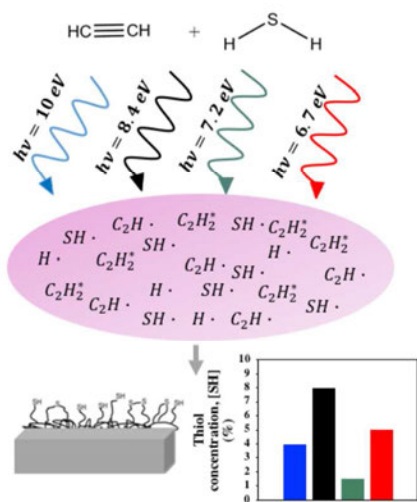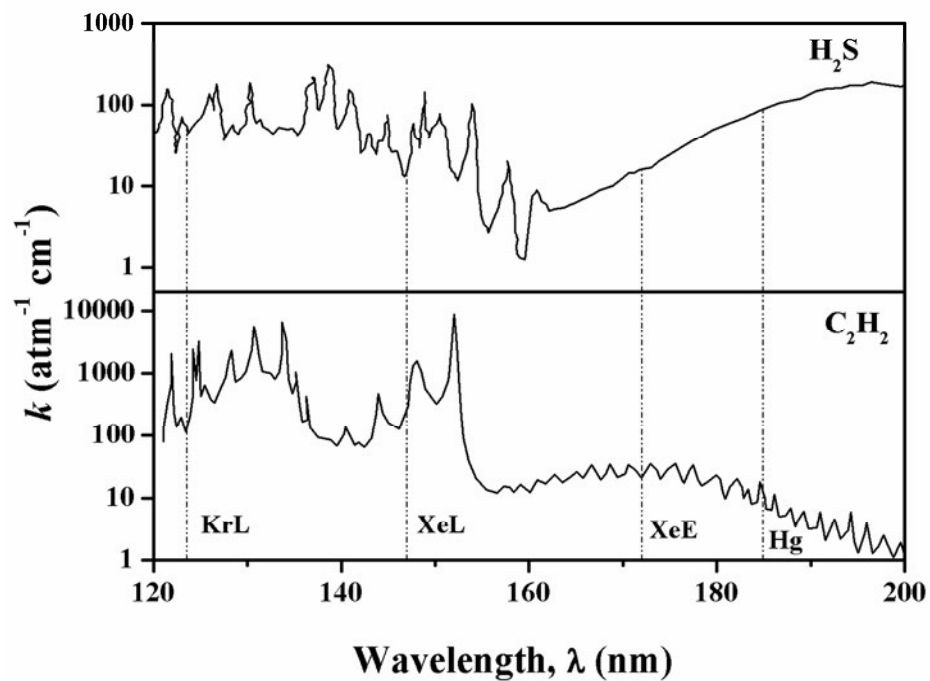
Figure 1. VUV-absorption, k (atm-1cm-1, base e) of gaseous H2S33 and C2H234; the wavelengths, λ, of the VUV lamps used are also shown (λKrL = 123.6 nm, λXeL = 147.0 nm, λXeE = 172.0 nm, λHg = 184.9 nm).
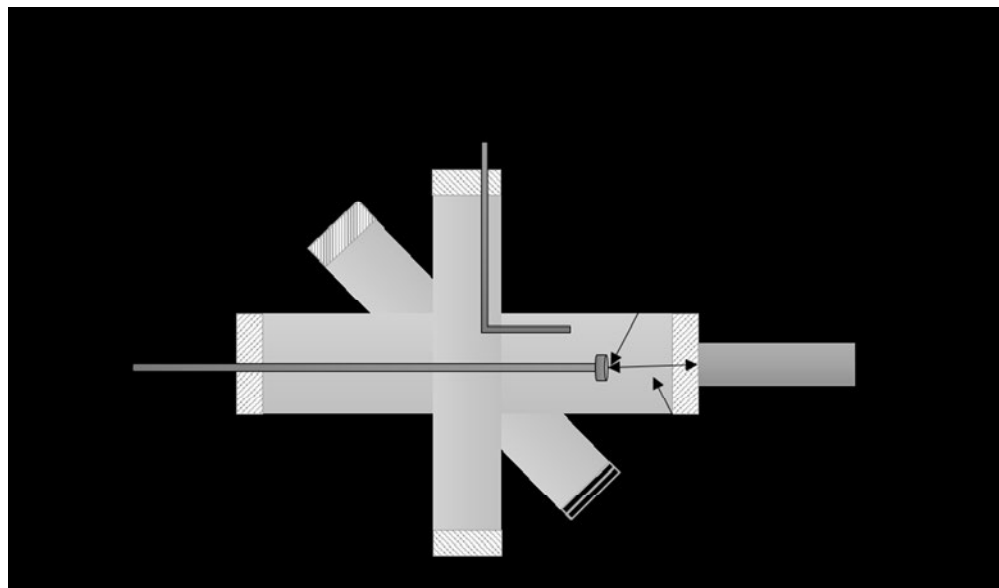
259x198mm (150 x 150 DPI)

Figure 2. Cross section of the vacuum ultra-violet (VUV) photo-chemical reactor chamber used for depositing thiol-terminated organic thin films.
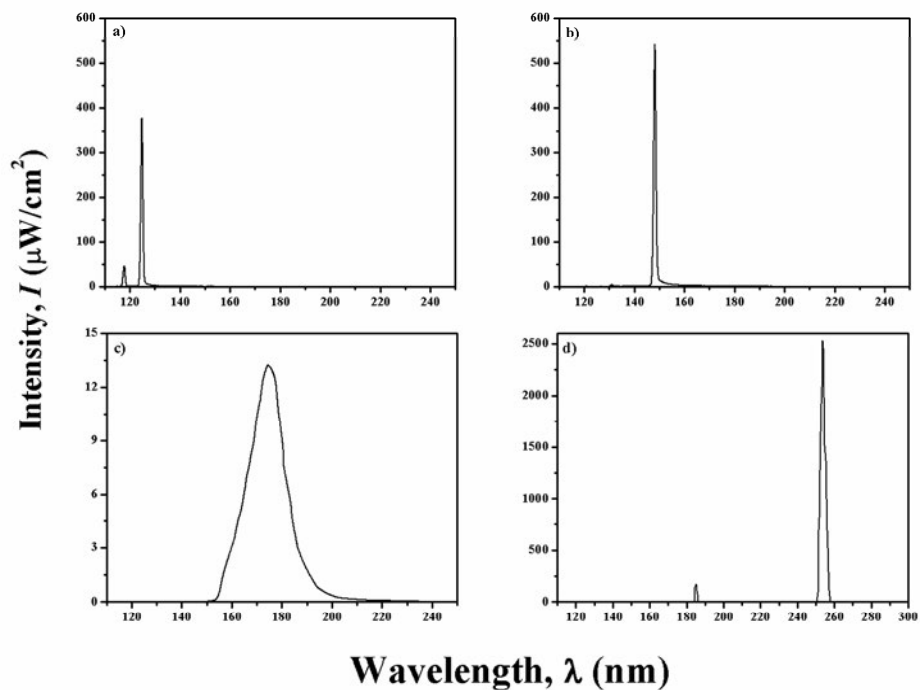
175x102mm (150 x 150 DPI)

1
2
3
4
5
6
7
8
9
10
11
12
13
14
15
16
17
18
19
20
21
22
23
24
25
26
27
28
29
30

Figure 3. Intensities and spectral distributions of the VUV radiation emitted by the a) resonant Kr; b) resonant Xe; c) Xe excimer (as measured by Truica et al.27-28, 32 at d = 6.0 cm under high vacuum); and d) Hg lamps (spectrum obtained from the manufacturer, corresponding to d=5.08 cm48 in air).

259x198mm (150 x 150 DPI)
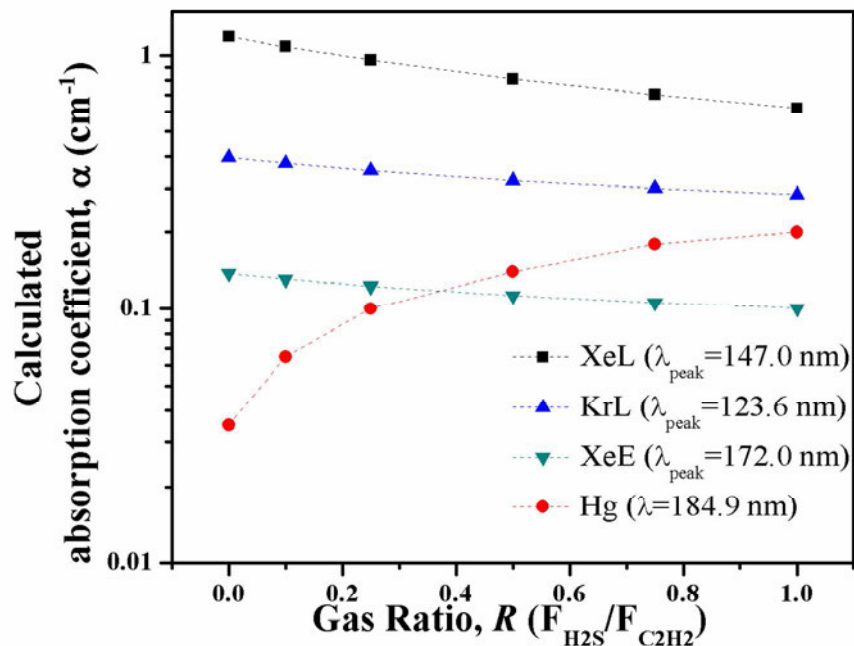
31
32
33
34
35
36
37
38
39
40
41
42
43
44
45
46
47
48
49
50
51
52
53
54
55
56
57
58
59
60

Figure 4. Calculated absorption coefficients, α (in cm-1), calculated using equation (7) for H2S/C2H2 gas mixtures; the corresponding wavelengths are those of the XeL (squares), KrL (triangles), XeE (upside down triangles), Hg (circles) VUV sources.
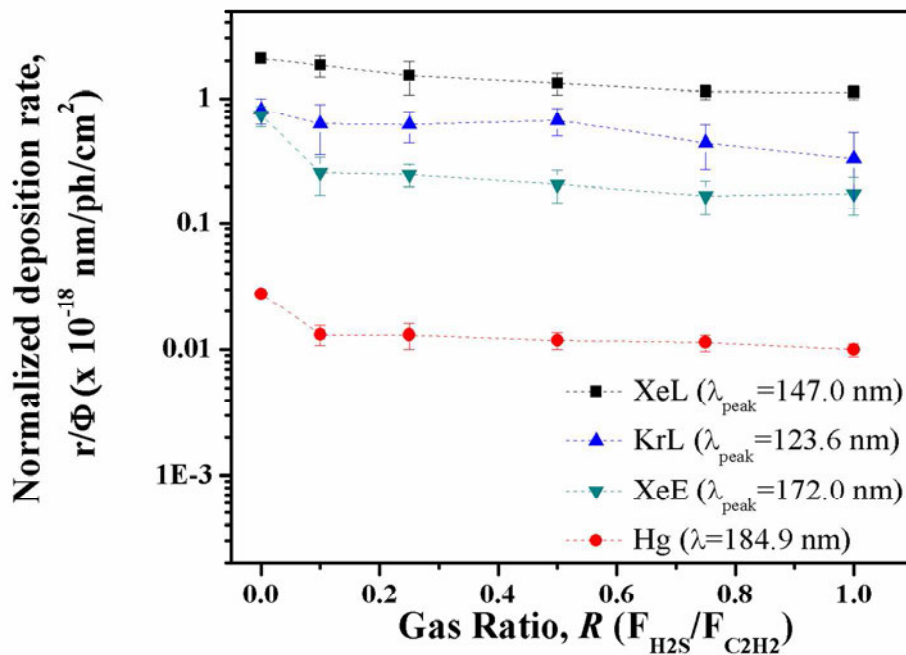
259x199mm (150 x 150 DPI)

Figure 5. Normalized deposition rates, r/Φ, as a function of gas mixture ratio, R, for UV-PA:S films deposited using the XeL (squares), KrL (triangles), XeE (upside down triangles), Hg (circles) sources. Error bars indicate 95% confidence interval. The lines are to guide the reader's eye.
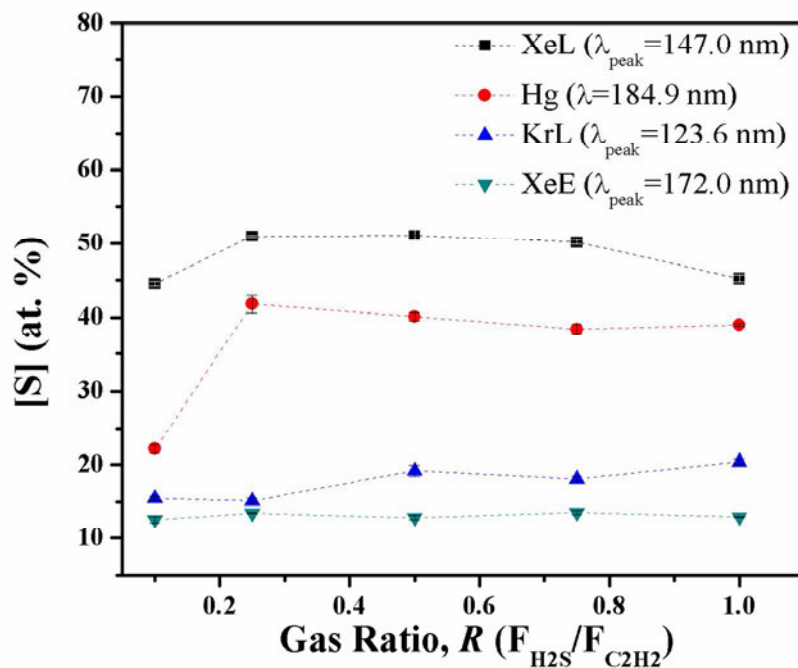
259x199mm (150 x 150 DPI)

Figure 6. Sulfur concentrations, [S] (in at.- %) of UV-PA:S films deposited using XeL (squares), KrL (triangles), XeE (upside down triangles), Hg (circles) VUV sources, as a function of gas mixture ratio, R. The lines are to guide the reader's eye.
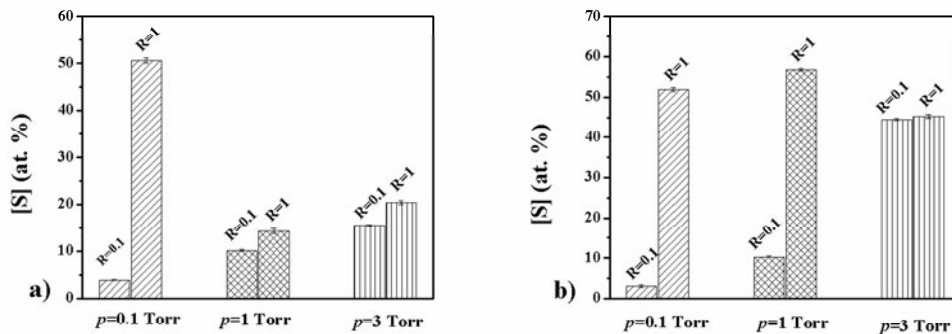
259x199mm (150 x 150 DPI)

1
2
3
4
5
6
7
8
9
10
11
12
13
14
15
16
17
18
19
20
21
22
23
24
25
26
27
28
29
30
31

Figure 7. Sulfur concentrations, [S] (in at.- %), for UV-PA:S films deposited using the a) KrL and b) XeL VUV sources at three different pressures (p=0.1, 1 and 3 Torr) and two gas mixture ratios (R=0.1 and 1).
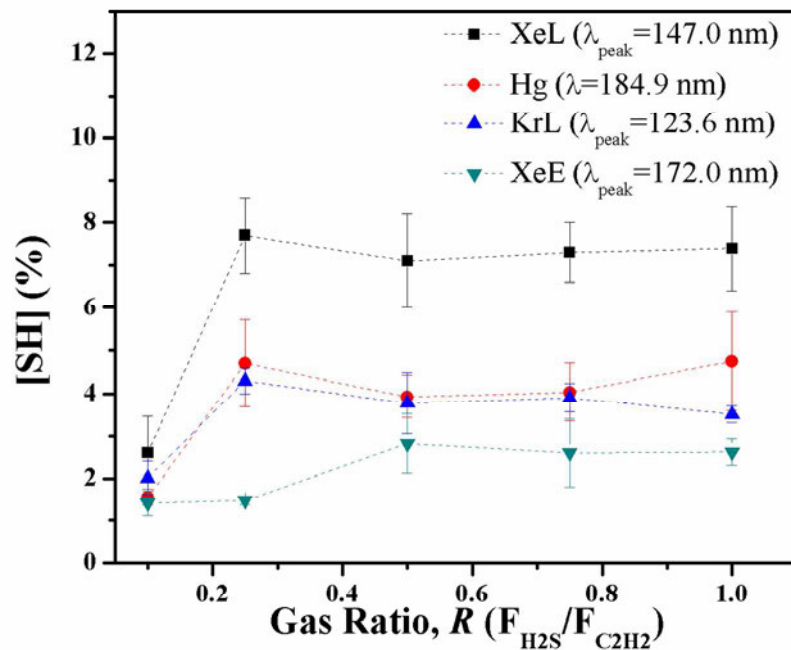
259x198mm (150 x 150 DPI)

32
33
34
35
36
37
38
39
40
41
42
43
44
45
46
47
48
49
50
51
52
53
54
55
56
57
58
59
60

Figure 8. Proportion of C bearing -SH groups, [SH] (in %), determined using chemical derivatization XPS for UV-PA:S films based on XeL (squares), KrL (triangles), XeE (upside down triangles), Hg (circles) VUV sources, versus gas mixture ratio, R. Error bars show standard deviations of three measurements. The lines are to guide the reader's eye.
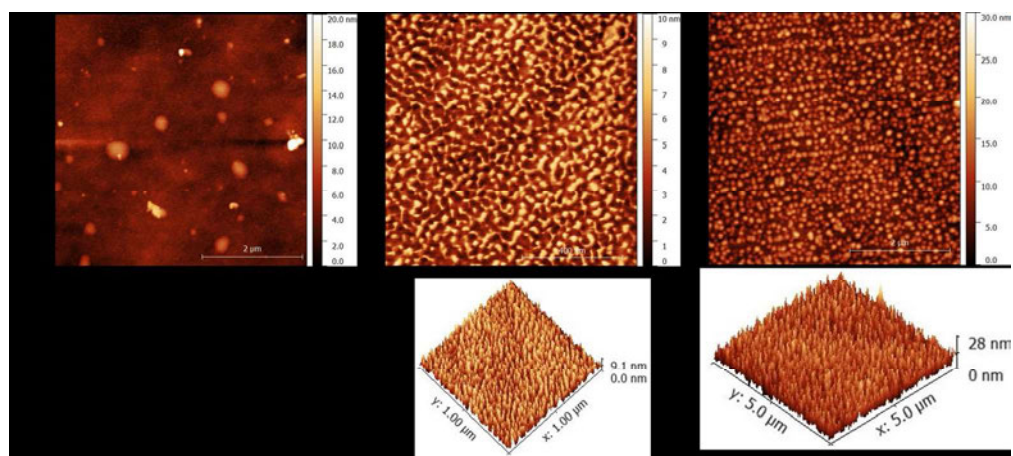
259x199mm (150 x 150 DPI)

Figure 9. Atomic force microscopy topography images of UV-PA:S films deposited using the KrL VUV source at a) R=0.1 (5x5 µm2); b) R=0.1 (1x1 µm2); and (c) R=1 (1x1 µm2). The bottom images represent 3D portrayals of the respective surfaces.
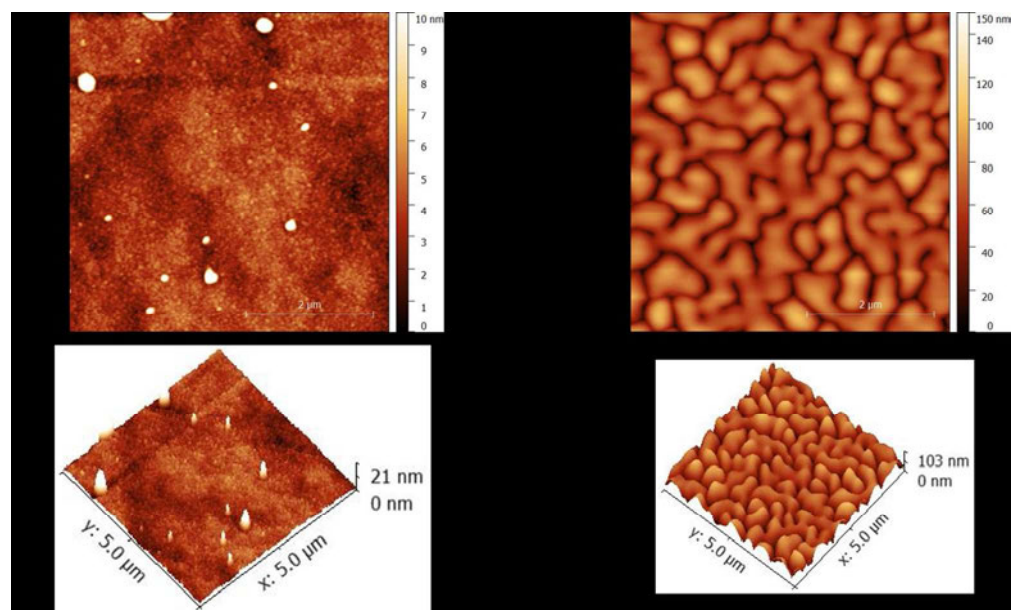
Figure 10. Atomic force microscopy topography images of UV-PA:S films deposited using the Hg VUV source at a) R=0.1 (5x5 μm2); and b) R=1 (5x5 μm2). The bottom images represent 3D portrayals of the respective surfaces.